Optical performance and results from the alignment and testing of the cameras for the MOONS spectrograph

Martin Fisher, Martin Black, David King, David Lee, Ian Parry, et al.

Published version information:

Citation: M Fisher et al. Optical performance and results from the alignment and testing of the cameras for the MOONS spectrograph.. Proc SPIE 12184 (2022): 121846W. Is in proceedings of: Conference on Ground-Based and Airborne Instrumentation for Astronomy IX, Montreal, CANADA, 17-22 Jul 2022

DOI: 10.1117/12.2629279

Optical performance and results from the alignment and testing of the cameras for the MOONS spectrograph.

Martin Fisher, Martin Black, David King, David Lee, Ian Parry, et al.

Martin Fisher, Martin Black, David King, David Lee, Ian Parry, Xiaowei Sun, "Optical performance and results from the alignment and testing of the cameras for the MOONS spectrograph.," Proc. SPIE 12184, Ground-based and Airborne Instrumentation for Astronomy IX, 121846W (29 August 2022); doi: 10.1117/12.2629279

SPIE.

Event: SPIE Astronomical Telescopes + Instrumentation, 2022, Montréal, Québec, Canada

Optical performance and results from the alignment and testing of the cameras for the MOONS spectrograph

Martin Fisher[1], Martin Black[2], David King[3], David Lee[2], Ian Parry[3] and Xiaowei Sun[1]
[1] University of Cambridge, Cavendish Laboratory, [2] UK Astronomy Technology Centre, [3] University of Cambridge, Institute of Astronomy

ABSTRACT

The MOONS (Multi-Object Optical and Near-infrared Spectrograph) is a twin, fibre-fed spectrograph for the VLT. Each spectrograph is fed with 512 fibres, the light from which is dispersed into three arms covering the RI, YJ and H bands. A separate camera is provided for each band, requiring six cameras to be produced and individually aligned. All six cameras have been assembled, aligned and cryogenically tested. The RI and YJ cameras, have been successfully integrated into the MOONS instrument cryostat and two more, including at least one of the H-band cameras are expected to be fitted for the next cool-down. Following an overview of the optical design of the camera, this paper presents the mechanical design together with stray light analysis and the inclusion of baffling. Six sets of optics have been provided by Bertin Winlight and an overview of their metrology data is presented. After assembly and pre-alignment of the first set of optics into the camera housing, a series of static and dynamic tests were carried out to ensure that the optics would remain in alignment following handling, transportation and ESO specified earthquake conditions. The pre-alignment stage and subsequent mechanical tests are described together with results from displacement and impulse testing. Because of the steep aspheric surfaces of the camera optics each set must be aligned in tilt and de-space at cryogenic temperatures. The facility specifically designed to accommodate the cryogenic alignment and stability testing of the MOONS cameras is presented and the fine alignment process under both warm and cryogenic conditions is described. Results from the final alignment stage and the stability of alignment under cryogenic cooling are presented and discussed.

Keywords: Ground-based instruments, multi-object infrared spectrographs, cryogenic alignment and testing, stray light analysis.

1 INTRODUCTION

This paper is split into six further sections covering the work carried out to produce, align and test the six cameras that the MOONS spectrograph requires to populate the arms of its twin arrangement. In section 2 the optical arrangement of the MOONS cameras is described, including an overview of the camera optical design. Section 3 provides an outline of the mechanical design of the camera which will aid appreciating the test method and results obtained. Section 4 covers metrology data of the optical components and stray light control within the camera. Section 5 describes the test facility and cryogenic vacuum chamber in which the MOONS camera is aligned at its operating temperature. Section 6 presents the alignment principle and stages undertaken to assemble and pre-align the camera optics before final alignment together with a summary of the optical test results for each of the six cameras. Finally, the seventh section presents the test method used to check the optical element alignment compliance under gravitational load changes and also the stability of the optical alignment under impulse loading to demonstrate its resilience to transport shocks and specified earthquake loads.

2 THE MOONS SPECTROGRAPH CAMERAS

2.1 Spectrograph arrangement and principal parameters

The baseline designs and description of the Multi-Object Optical and Near-infrared Spectrograph (MOONS) and options for the cameras has been presented previously [1,2]. The final design is two identical spectrographs, each collecting light from 512 fibres, collimated using a spherical mirror and fed via two dichroics to three dispersing elements and three cameras. The cameras cover three wavebands – RI, YJ and H – one of each for each spectrograph. Both low (R~4500) and high (R~9000-19000) resolution modes are used; RI and H use both modes, YJ uses low resolution in each spectrograph.

Ground-based and Airborne Instrumentation for Astronomy IX, edited by Christopher J. Evans, Julia J. Bryant, Kentaro Motohara, Proc. of SPIE Vol. 12184, 121846W
© 2022 SPIE · 0277-786X · doi: 10.1117/12.2629279

The spectrographs are housed in a cryogenic chamber, running at approximately 128 K. The main parameters of the MOONS spectrographs are shown in Table 1.

The camera design used in the MOONS spectrograph is the f/0.95 Wonder-Camera[2], a reflective camera which comprises only three elements: two fused silica lenses and a Clearceram-Z mirror. The mirror surface is aspheric. The first lens L1 is a meniscus lens with an aspheric front surface and spherical rear surface, and a central rectangular aperture which accommodates L2, the second lens, and the detector package which is mounted from a separate adjustment module bolted to the front of the camera. The front surface of L2 is aspheric and the rear surface planar. This arrangement simplifies the mounting and interfacing of the two lenses. The back focal distance is quite large, enabling filters to be installed between the rear of L2 and the detector – RG glasses for the RI and YJ cameras and Silicon for the H cameras.

Table 1 MOONS spectrograph main parameters

Sky projected fibre diameter	ϕ_{fib} = 1.0 arcsec
Collimator focal ratio	F_{coll} = 3.5
Fibres per spectrograph	N_{fib} = 512
Input slit length	L_{slit} = 200 mm
Collimated beam diameter	D_{coll} = 265 mm
Camera focal ration	F_{cam} = 0.95
Sampling	N_{res} = 2.7 pix (40.5 µm)
Dark Pixels between fibres	N_{dark} = 4.5 pix
Detector and pixel size	NX_{pix} = 4096, NY_{pix} = 4096, 15 µm pixels
Simultaneous Wavelength coverage and resolving power in LR mode	RI: 647 – 955 nm R=4500 YJ: 934 – 1350 nm R=4300 H: 1452 – 1800 nm R=6800
Simultaneous Wavelength coverage and resolving power in HR mode	RI: 765 – 897 nm R=9100 YJ: 934 – 1350 nm R=4300 H: 1523 – 1640 nm R=18800

2.2 Spectrograph layout and camera design overview

The layout of the spectrograph is presented in Figure 1 for the low-resolution configuration and in Figure 2 for the high-resolution configuration.

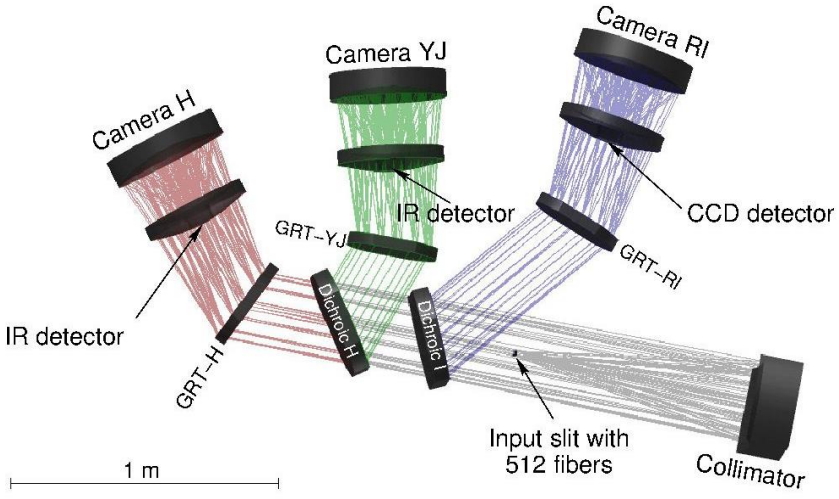

Figure 1 Spectrograph layout for the low-resolution configuration.

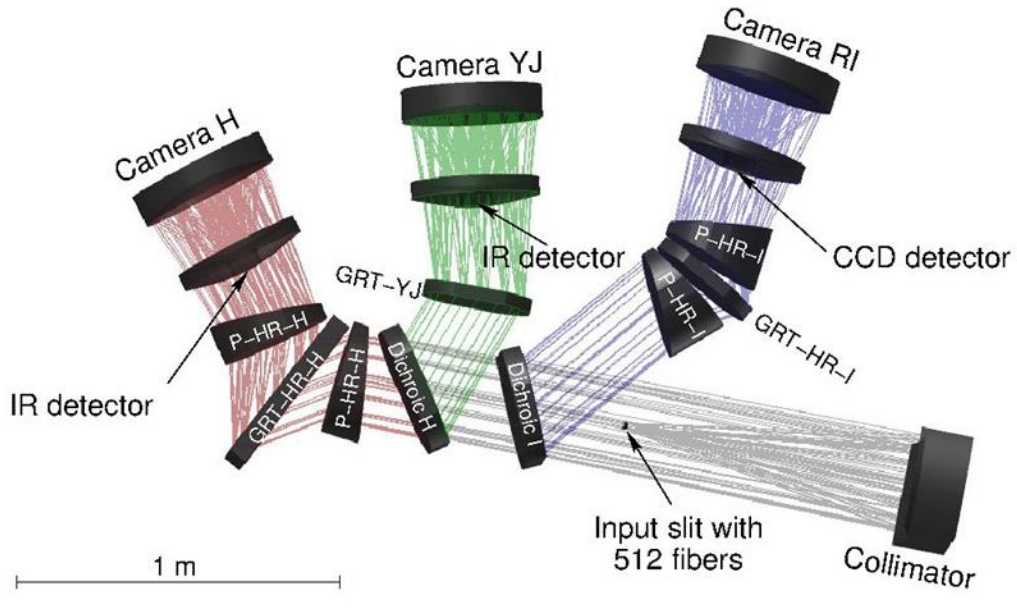

Figure 2 Spectrograph layout for the high-resolution H and RI configuration

The camera layout and optical quality is shown in Figure 3. The encircled energy diameter is shown at 50% (green), 80% (red) and 95% (blue) at different wavelengths and spatial positions along the slit.

The three cameras covering the three wavebands are very similar, having slightly different optical prescriptions optimised for each waveband, with small differences in surface curvatures and aspheric coefficients on the mirror and lens surfaces, and mirror to lens separation.

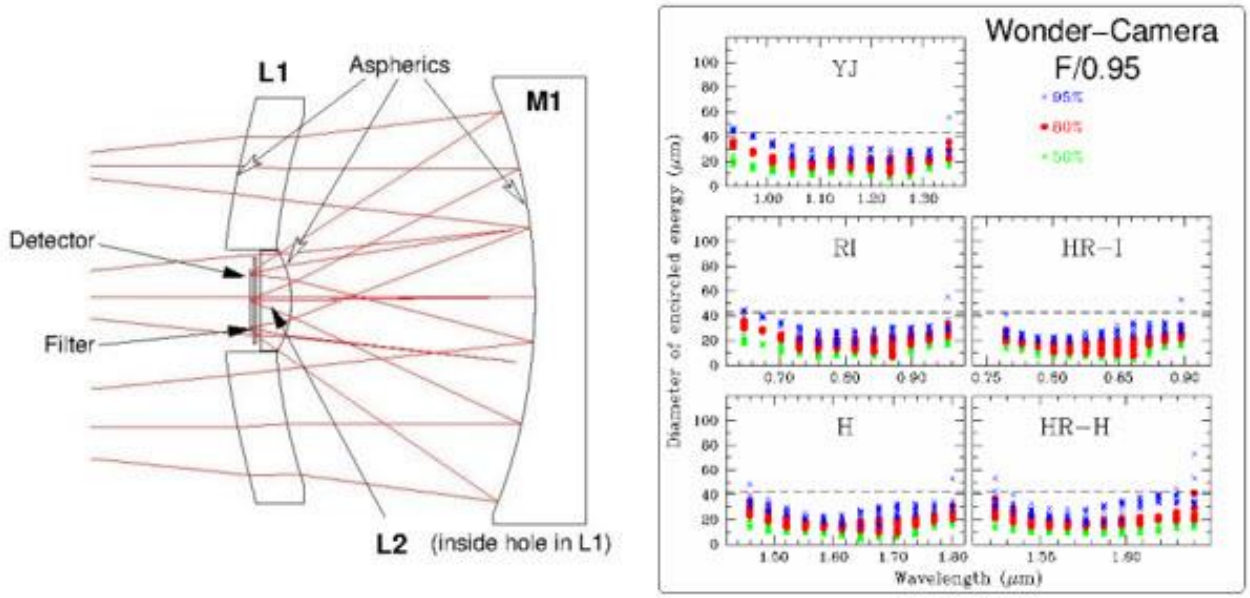

Figure 3 Left – Layout of the f/0.95 Wonder-Camera. Right – Optical quality of the f/0.95 Wonder-Camera.

3 CAMERA MECHANICAL DESIGN

The RI, YJ and H band cameras are mounted either side of a central optics bench of the spectrograph instrument cryostat with orientations of the optical axis at 98°, 76.4° and 52° respectively to the gravity vector. The camera detector is mounted on a Detector Adjustment Module which is not part of this deliverable but attaches to the front of the camera. All the cameras share a common mechanical design with the spacing between the lens and mirror elements adjusted according to the operating waveband and the variation due to manufacturing tolerances of the individual optics themselves. A model of the camera design is shown in Figure 4 and consists of the Mirror and Lens Modules, the support Barrel, Baffle Rings, three Flexure Mechanisms, and the Camera Support Structure.

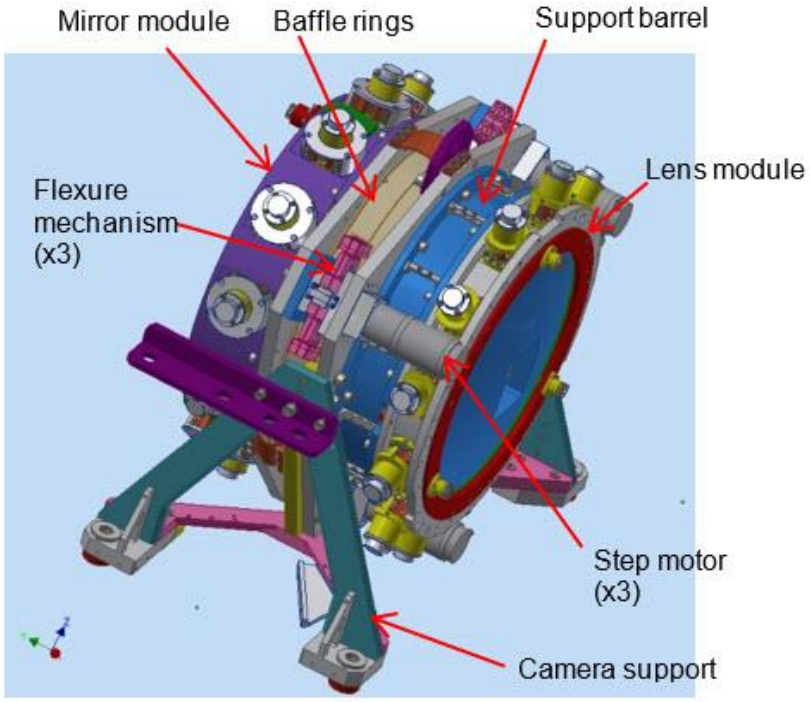

Figure 4 A 3-D model of the camera mechanical design

Each flexure mechanism consists of a specially designed titanium alloy flexure, a stainless-steel leadscrew drive and a geared stepper motor. This arrangement provides for both de-space and tilt adjustments of the mirror module with respect to the lens module at both room temperature and cryogenic temperatures thus allowing final alignment of the camera to be undertaken at the operating temperature of approximately 128 K. Exchangeable shims are used to account for the large change in de-space of the lens and mirror modules between warm and cold alignment stages. This is done so that the tilt of the mirror module is close to the alignment position and the shims machined such that each flexure then operates close to its un-flexed position. Another feature of this design is that, once brought back to room temperature, the mechanism can be locked and the motors removed for use on the next camera with minimal disturbance to the optical alignment of the camera. To assist in cooling the mirror module, flexible copper strapping is used to provide a thermal bridge to the barrel and lens assembly attached to the support structure. Cooling of the camera assembly is provided from the spectrograph optics bench via the support structure and additional thermal straps.

The lens assembly is mounted in the lens module such that it is defined and retained axially and supported radially by spring loaded radial support units. The Clearceram-Z mirror is specially machined so that it also can be defined and retained axially and is supported radially by radial support units similar to those used for the lens. This arrangement ensures that the lens and mirror are protected against shock loading and yet return to their nominal position so that camera alignment

remains within specifications. The lens support barrel can be positioned laterally so that the lens axis and mirror axis can be co-aligned in an integration stage before warm alignment of the complete camera. A photograph of the assembled camera is shown in Figure 5.

The design of the radial supports allows for the difference in the coefficient of thermal expansion between the aluminium material and optical material while also offering a thermal path to help with cooling of the optics. The stiffness of the radial respective supports is chosen so that the lens and mirror move by similar amounts under gravitational loading. This allows all cameras to be aligned in the horizontal position so that they remain within alignment specifications when they are mounted at their operation orientation.

The main material used for the optics modules and support structure is aluminium alloy. To achieve a thermally stable structure, the component parts of the modules and structures were stress-relieved before final machining. A specially selected black paint was applied on the baffles and some surfaces to achieve stray light reduction (see section 4.4).

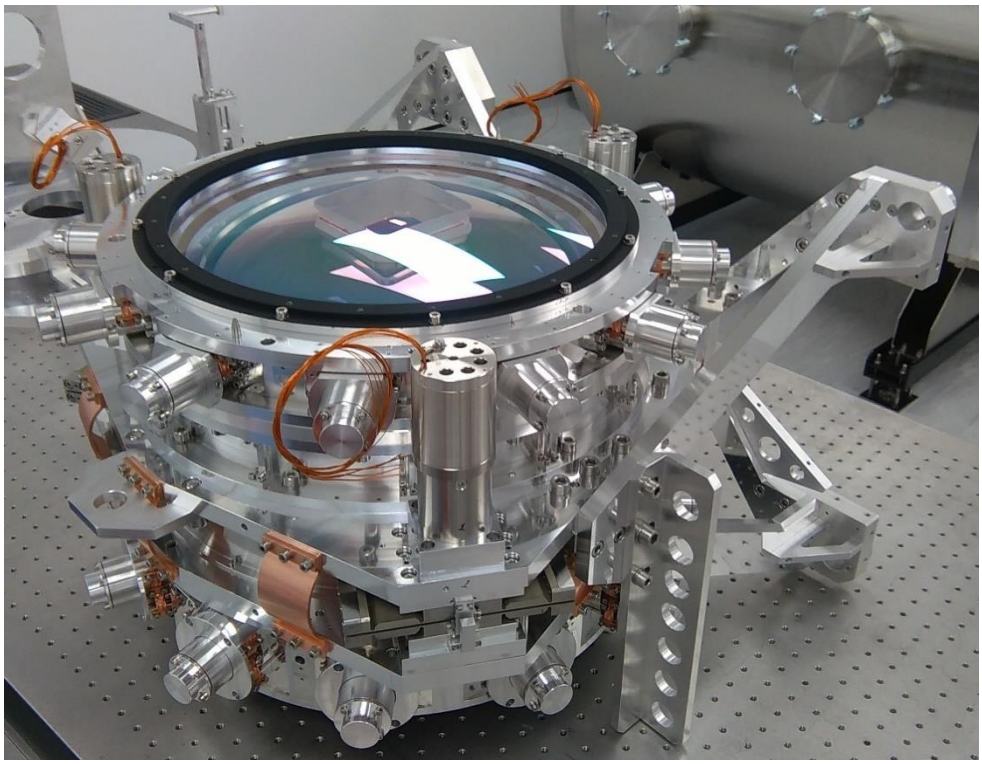

Figure 5 A photograph of an assembled camera (resting on its mirror cell) prior to warm alignment. The rectangular cut-out in the main lens is clearly visible as are the radial supports of the mirror cell module and the mirror cell. Also visible in the lower centre of the picture is a flexure mechanism with its motor-gearbox. Flexible copper strapping bridges the mirror cell module to the lens support module.

4 METROLOGY DATA AND STRAY LIGHT CONTROL

4.1 Dimensions

The optical specification for the MOONS camera optics: L1, L2, and the mirror, included a list of critical dimensions to be verified by the manufacturer, for all six cameras. These critical dimensions, such as lens thickness, need to be within the specified tolerances for the part to be accepted by the MOONS consortium. A full list of key dimensions was supplied by the manufacturer, demonstrating the parts meet requirements. These dimensions were used to update the camera Zemax optical design file so that the camera alignment proceeds using as-built dimensions. Knowledge of some other dimensions, such as lens diameter, were used to make minor adjustments to the lens mounts so that they are an exact fit to the manufactured optical components.

4.2 Surface form error

All optical surfaces, in all six MOONS cameras, were measured by the manufacturer, with an interferometric test setup, to determine surface form error. Surface form error maps were supplied to the MOONS consortium for further analysis and incorporation into the optical design files. An example surface form error map, for the YJ-band mirror serial number 1, is shown in Figure 6. The surface form error map shows the full 404 mm diameter clear aperture of the mirror. The reflected wavefront error over the nominal beam footprint of 270 mm diameter is typically less than 150 nm RMS.

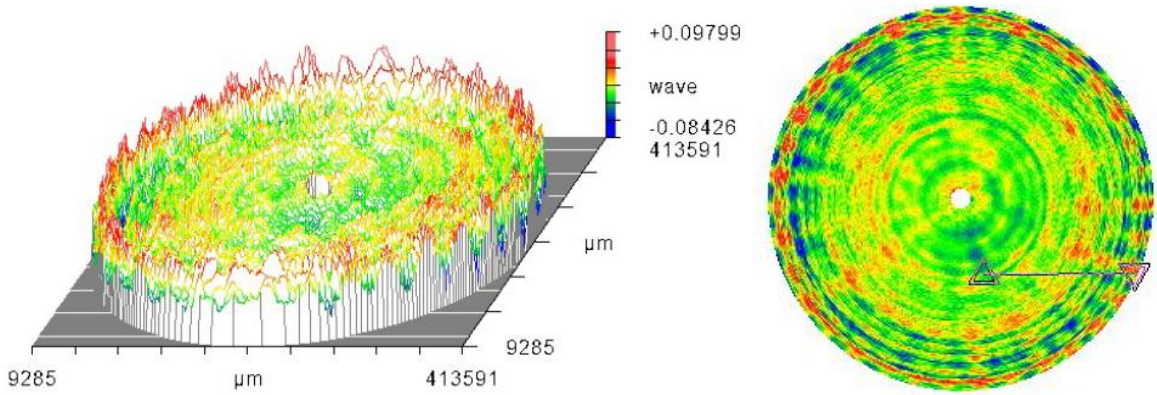

Figure 6. Plot of the measured surface form error for the YJ-band camera mirror, serial number 1, following the removal of piston, tilt, power, astigmatism, coma, and spherical terms. Measurement wavelength is 632.8 nm. The measured area on the mirror is 404 mm diameter. The magnitudes of the subtracted aberrations are: astigmatism 142 nm RMS, coma 1 nm RMS, and spherical 8 nm RMS.

4.3 Coating performance

The three different types of MOONS camera, RI-band, YJ-band, and H-band, have slightly different optical coatings optimized for the wavelength range of operation. The lenses are coated with multi-layer anti-reflection coatings, see Figure 7, and the mirrors have silver metallic coating see Figure 8. A summary of the optical performance of each type of coating is given in Table 2. All coatings meet the requirements as per the MOONS throughput budget.

Table 2 Summary of the performance of the MOONS camera optical coatings for unpolarized light.

Component and type of coating	**Wavelength range**	**Achieved coating performance**
Lenses 1 and 2, RI-band, anti-reflection coating, angles of incidence 0 - 40°	640 – 950 nm	Average reflectivity < 0.57 %
Lenses 1 and 2, YJ-band, anti-reflection coating, angles of incidence 0 - 40°	940 – 1350 nm	Average reflectivity < 0.49 %
Lenses 1 and 2, H-band, anti-reflection coating, angles of incidence 0 - 40°	1450 – 1800 nm	Average reflectivity < 0.41 %
Mirrors, all-bands, reflective coating	640 – 950 nm 940 – 1350 nm 1450 – 1800 nm	Average reflectivity > 97.6 % Average reflectivity > 98.6 % Average reflectivity > 99.4 %

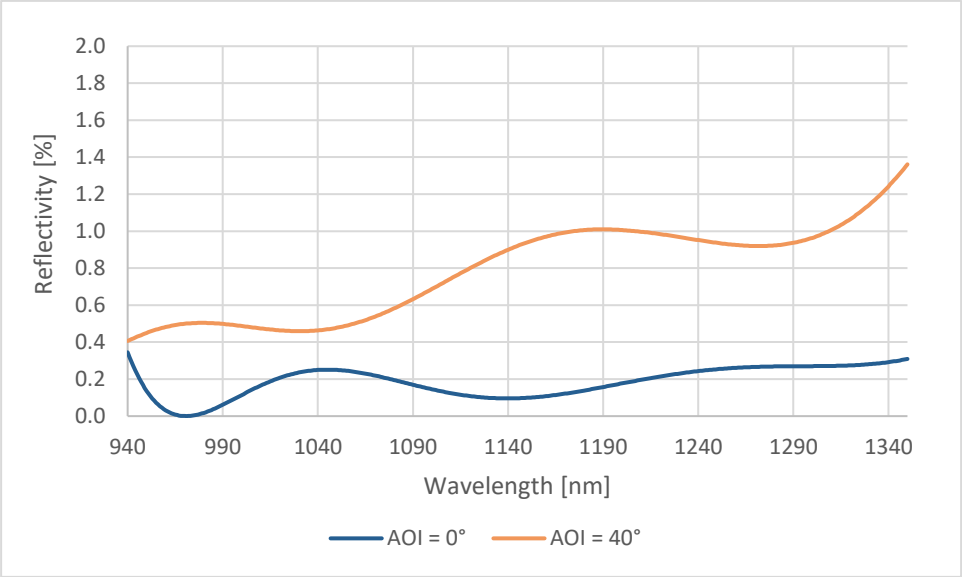

Figure 7. Plot of the measured reflectivity versus wavelength for the YJ-band L1 concave surface.

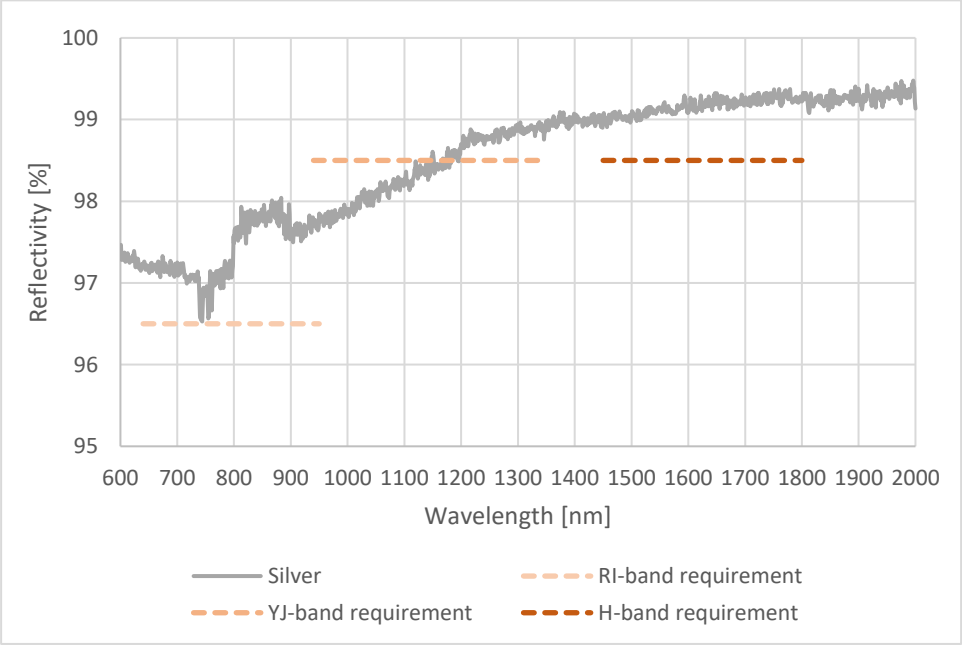

Figure 8 Plot of the measured reflectivity versus wavelength of the MOONS camera's silver mirror coating.

4.4 Camera baffles

A feature of the MOONS camera opto-mechanical design is that the smaller L2 is mounted in a cut-out aperture inside the larger L1, Figure 9 Left. L2 is bonded to a mounting area that is directly machined into the fused silica material of L1. This optically transparent L1 to L2 interface region would allow stray-light to reach the detector unless an appropriate baffle is fitted. The left-hand picture in Figure 9 shows the front of L1 and the approximately square mounting area for L2 can be seen in the centre and L2 itself can be seen in the centre. This area is baffled using a black painted baffle fitted to the detector mount, as can be seen in the right-hand picture in Figure 9. The vertical edges of the L1 – L2 baffle, and the detector mounting spiders, are fitted with a triangular profile, or zig-zag pattern. This edge pattern causes the spider's

diffraction pattern at the detector to be inclined at ± 10 degrees with respect to the spectrum. This reduces the amount of diffracted stray light from bright hydroxyl (OH) emission lines in the spectrum of the fainter scientific targets, Li Causi et al. 2016[3].

The camera also features more traditional annular baffles to block stray-light paths at the edges of lenses and mirrors. The left-hand picture in Figure 9 shows the black painted annular baffle at the edge of L1. The right-hand picture in Figure 9 shows a second annular baffle fitted to the detector adjustment module to provide a further layer of baffling. There is a further annular baffle located inside the camera barrel that prevents light reaching the edge of the mirror.

In general, the coating used for the MOONS baffles is Aeroglaze® Z306 flat black paint except in some critical areas, such as near the detector, where Acktar Vacuum Black™ is used instead. The use of Acktar coating near the detector eliminates the small risk associated with loose flecks of paint falling on the detector surface. The lower reflectivity of the Acktar coating compared with Aeroglaze® black paint is noticeable in the right-hand picture in Figure 9.

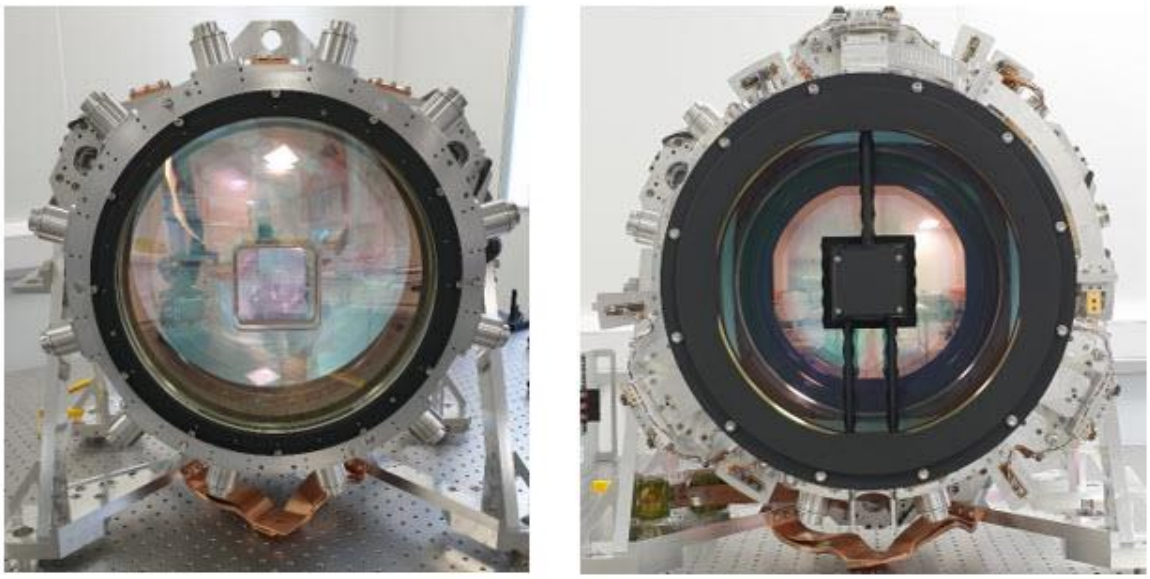

Figure 9 **Left** – picture of the MOONS H-band camera barrel showing L1, with the square central aperture where L2 is mounted. **Right** – H-band camera with the detector adjustment module fitted. The central L2 baffle, spider baffles, and outer baffle will prevent stray-light paths.

5 CAMERA CRYOGENIC TEST FACILITY

5.1 Cryogenic vacuum chamber

Assembly of the MOONS cameras took place in an ISO 7 cleanroom at the Cavendish Laboratory of the Department of Physics, University of Cambridge, U.K.

For the cold alignment stage of the MOONS cameras, a cryogenic test facility was designed to accommodate the optical test bench, comprising a MOONS collimator, an optical test arrangement and the camera assembly. The vacuum chamber with the necessary ports was commissioned from Kurt J Lesker in the UK. The chamber was then fitted out with a radiation shield, an internal liquid nitrogen dewar (which can be filled in situ), copper strapping and a set of rails that would carry the purpose designed bench on which the complete optical test arrangement would fit. The bench is supported by wheels so that the test arrangement can be constructed on a trolley outside of the chamber and fitted with the camera to be tested, which then undergoes a warm alignment process described later. Following warm alignment, the test bench is rolled into the chamber and thermal straps and electrical connections are made before closing the door. A photograph of the chamber with the test bench and a mounted camera is shown in Figure 10 (left). The chamber is pumped down for a day and then liquid nitrogen is introduced through a vacuum port to the rear of the internal dewar. Nitrogen vapour is allowed to escape

through a vent port at the top of the chamber and a safety valve is fitted to the chamber in the (very unlikely) event of a nitrogen leak into the chamber itself.

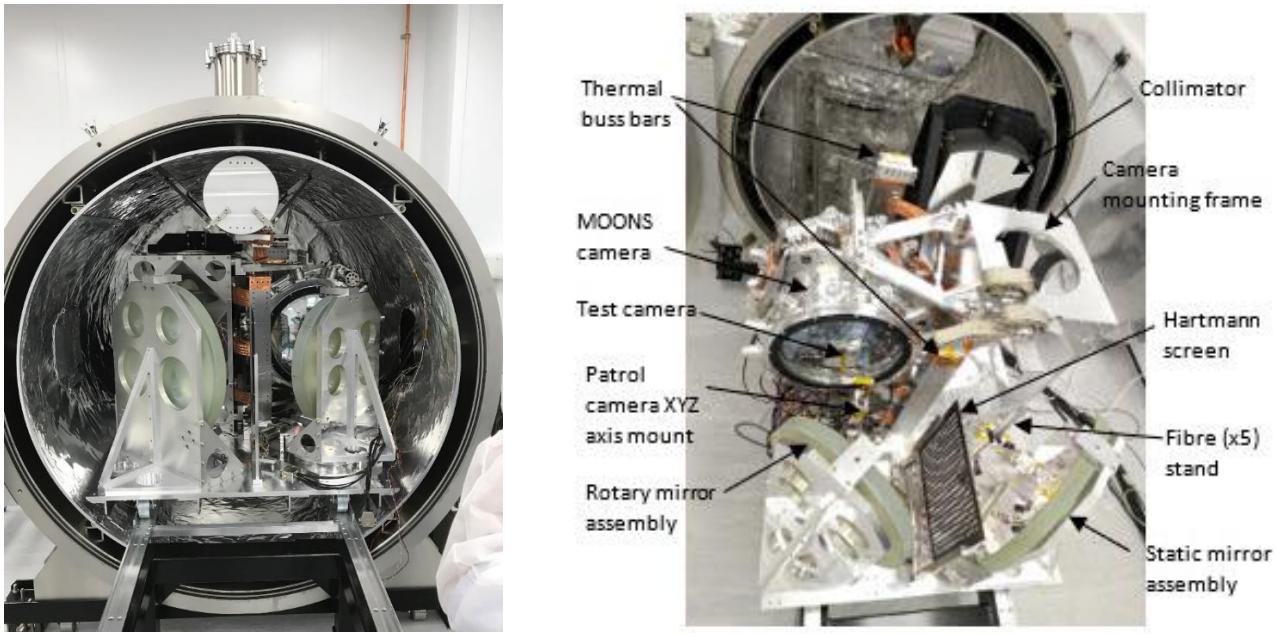

Figure 10 **Left**, the cryogenic test chamber with the optical test arrangement on the wheeled platform inserted. **Right**, the MOONS camera test bench re-configured for the last three cameras.

The chamber, the test bench and the camera are fitted with PT100 sensors at various locations of interest so that the cool-down process can be monitored. Cooling down generally takes about eight days but requires a day or two more for the camera optics to stabilise.

5.2 Camera test arrangement

The camera test bench is described more functionally in a later section. It comprises a MOONS collimator fed by a set of five optical fibres in the form of a sparsely populated slit, a large fold mirror, a Hartmann screen, a rotatable fold mirror and a MOONS camera mounted on a support frame as it would be in the MOONS instrument cryostat except that its optical axis is horizontal. An XIMEA miniature camera on a purpose-built XYZ stage is able to 'patrol' the focal plane of the camera i.e., inside the cut-out of the lens. This arrangement allows the slit to be imaged across the full field of the camera. A photograph of the test bench is shown in Figure 10 (right).

The test bench is optically aligned before the first camera is fitted and remains as illustrated in Figure 10 (left) for the alignment of the first three MOONS cameras. The test bench is then reversed L-R Figure 10 (right), so that the next three cameras can be mounted as they would be in the MOONS instrument cryostat (on the other side of its optical bench). This ensures that all cameras are aligned under reasonably close gravitational loading to their actual operating orientations.

5.3 Test control electronics

The camera is fitted with three stepper motors and associated limit switches. The XIMEA miniature camera and the rotating mirror are also motorised. These mechanisms are also driven by stepper motors and have associated limits. There are no encoders and so step-counting is used to position these stages. For convenience and ensuring the centre position of the field is known, an optical sensor is used to detect a single 'reference' line on the X stage of the XIMEA camera. The cables for these mechanisms and sensors, including the USB connection of the miniature camera, are connected to vacuum rated through-connectors mounted in a side port of the chamber. These connections are taken to an electronics control crate

which houses power supplies, stepper motor drivers and a PMAC motion controller, PT100 modules and a Labjack interface. A PC running Windows 10 and various programs are used to control and monitor the alignment test.

6 CAMERA ALIGNMENT AND RESULTS

6.1 Introduction

Theoretically the alignment of the Wonder-Camera is simple, as it has only 3 elements with low thermal expansion coefficients. The two fused silica lens act as one element and the mirror as another, thus reducing the complexity of alignment. Moreover, changes of refractive index with temperature does not affect the optical quality; i.e., the camera can perform equally well at both room and cryogenic temperatures.

The optics for all six cameras were made by Bertin Winlight. Alignment and bonding of L2 to L1 was also performed by Bertin Winlight, and the L1/L2 combination supplied as a single element with the two lenses cemented together. This alignment procedure is not discussed further here. The relevant numbers from this procedure are shown in Table 3.

Table 3 Concentricity of the L2 aspheric surface Z axis (Z-L2) with respect to the L1 aspheric Z axis (Z-L1) and perpendicularity of the L2 flat surface with respect to the L1 aspheric surface Z axis (Z-L1)

Camera	Concentricity Z-L2 to Z-L1 /asph. surf. quad sum	Concentricity Z-L2 to L1 / asph. surf. linear sum	L2 flat surf. perp. to L1 Z axis asph. surf. quad sum	L2 flat. surf. perp. to L1 Z axis asph. surf. linear sum
Requirement	<0.2 mm/Z-L1	<0.2mm/Z-L1	⊥<2 arcmin / Z-L1	⊥<2 arcmin / Z-L1
H s/n 1	0.057 mm	0.085 mm	18 arcsec	25 arcsec
H s/n 2	0.029 mm	0.048 mm	24 arcsec	32 arcsec
RI s/n 1	0.024 mm	0.040 mm	67 arcsec	85 arcsec
RI s/n 2	0.024 mm	0.040 mm	22arcsec	31 arcsec
YJ s/n 1	0.044 mm	0.076 mm	33 arcsec	47 arcsec
YJ s/n 2	0.035 mm	0.055 mm	28 arcsec	40 arcsec

The baseline Zemax model for each camera was updated with the as-made optical parameters as measured by Bertin Winlight. These Zemax models were then re-optimised by changing the mirror to lens separation to deliver the best performance at operating temperature.

Table 4 summarizes the required positioning and stability tolerances of the optical elements within the camera. The tolerances are here defined as the displacements and tilts that produce an increase of only 7% of the error-function. The first row is the accuracy of the initial mounting (gluing) of L2 inside L1: the large tolerance in Delta-Z (shift along the optical axis) can be corrected by changing the distance between the L1/L2 and M1 during the re-optimisation. Rows two and three are the displacements from the aligned positions that can be recovered by tilting and refocussing the detector at operating temperature.

Table 4: Positioning and stability tolerances of the camera elements.

Elements	Compensators	Delta-Z	Delta-X/Y	Tilt
L2 rel. L1 (initial mounting/bonding)	M1 and detector	0.3mm	0.1mm	120 arcsec
L2 rel. L1 (stability after mounting)	Detector	0.05mm	0.1mm	60 arcsec
M1 rel. L1/L2	Detector	0.05mm	0.05mm	30 arcsec
Filter rel. to detector	None	1mm	5mm	1 degree
Camera rel. to disperser	Detector	5mm	1mm	6 arcmin

From here on the L1/L2 combination is simply referred to as the “lens”. Five degrees of freedom impact on the camera performance: x-tilt, y-tilt, x-decentre, y-decentre, and z-position of the lens to the mirror. Decentres are dealt with in the mechanical assembly of the MOONS cameras. Discussed here is the mutual alignment of the lens relative to the mirror within the camera body. The centring of the lens onto the mirror is by small lateral displacements of the lens module assembly. Tilts are achieved using three cryogenic adjustment mechanisms, with a resolution of 0.016 µm per micro-step. Total range on each mechanism is ~2.7 mm.

The alignment and testing of the MOONS cameras proceeded as follows:

- Preliminary mutual alignment on the optical bench of the mirror and lens using laser back-reflections.
- Alignment in the purpose-built test bench at both ambient and cryogenic temperature, using one of the MOONS spectrograph collimator mirrors. The tilts and spacings are adjusted using the three cryogenic mechanisms both at ambient and cryogenic temperatures. The test bench is placed inside a purpose-built vacuum chamber for the cryogenic alignment and test procedures.

6.2 Preliminary optical bench alignment

The layout of the optical bench alignment is shown in Figure 11.

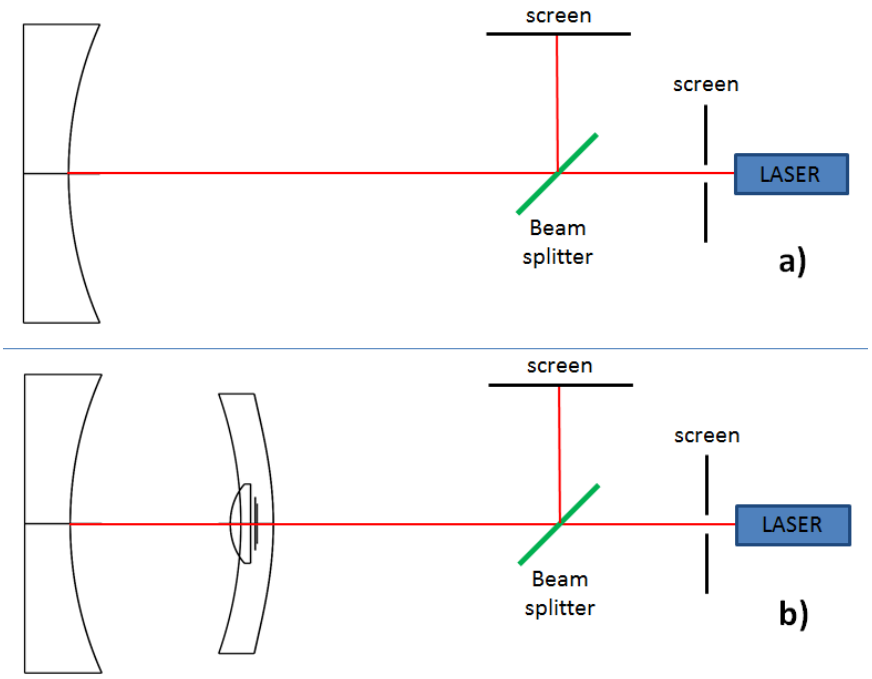

Figure 11 Optical setup for the preliminary alignment of the camera; a) the optical axis of the mirror is defined by the laser beam. The mirror is adjusted in X and Y so the return beam is coincident with the input beam. b) the lens is added so that its back reflections coincide with that of the mirror. Note that this arrangement was modified to put the camera optics upward facing by including a fold mirror between the laser and beam splitter.

Spacers were manufactured for each camera to match the mirror to lens spacing as determined from the re-optimisation of each camera’s Zemax optical model, so that when each camera is assembled the tilt/piston adjusters were in mid-range (see description in mechanical section).

Note that the alignment arrangement shown in Figure 11 was altered by including a fold mirror prior to the beam splitter, so the camera would be upward facing on the optical bench. The laser beam defines the optical axis. Both the mirror and

lens were brought into alignment on this axis in a standard manner by viewing the back reflections from the optical surfaces. The mirror was centred first, followed by the lens.

6.3 Ambient and Cryogenic alignment on the test bench

The first camera (YJ camera s/n 1) went through several iterations at both ambient and cryogenic temperatures to refine the alignment and data analysis procedures. However, once the best methodology was determined, the additional five cameras proceeded more rapidly.

The alignment optical setup and detailed assembly are shown in Figure 12. The test bench comprises:

- The curved input slit. Five fibres are positioned symmetrically along the full slit length.
- The MOONS collimator mirror – this is the second of the two MOONS collimator mirrors.
- A fixed folding flat to fold the beam.
- The Hartmann screen.
- A rotating folding flat which mimics the dispersion grating by steering the beam in the "wavelength" direction.
- The MOONS camera under test.
- An XIMEA camera mounted on an XYZ stage to patrol the MOONS camera focal plane.

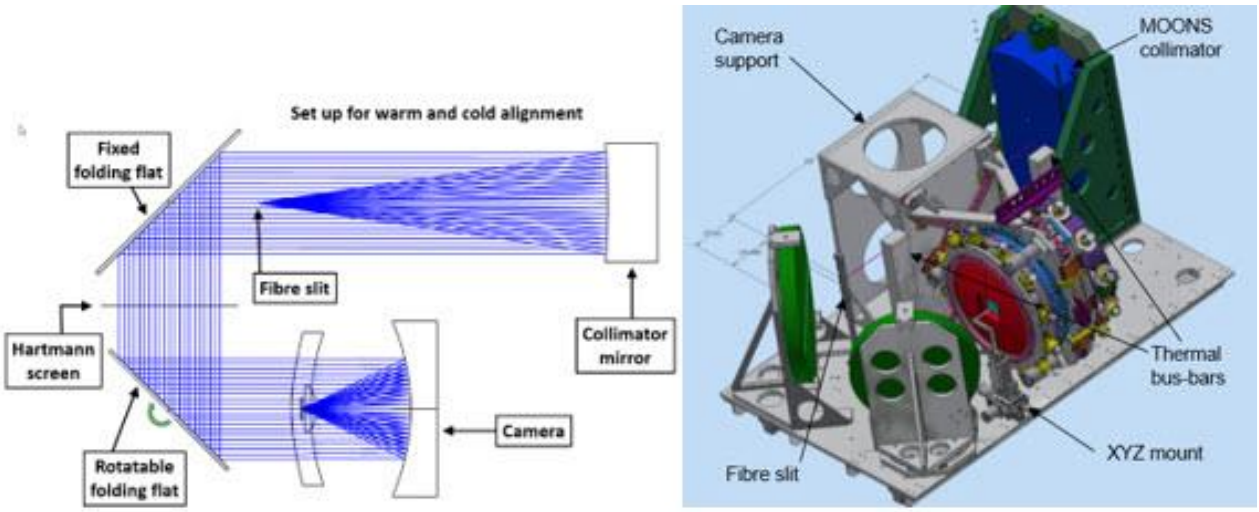

Figure 12: The optical setup and detailed assembly of the test rig, used for both ambient and cryogenic alignment procedures and collection of test data. The fibre slit comprises five fibres arranged symmetrically over the full slit length. The rotating fold mirror steers the beam to create images over the full width of the focal plane to mimic the wavefront tilt provided by the grating in the full spectrograph.

The input fibres are 150 microns diameter, equally spaced along the 200 mm curved slit, ensuring full coverage in the "spatial" direction in the final focal plane (61.5 mm x 61.5 mm). For all cameras the fibre inputs were illuminated using an 850 nm wavelength LED, irrespective of the design waveband of the camera. Images were recorded in the focal plane using an XIMEA CMOS camera (2592x1944, 2.2 µm pixels) mounted on an XYZ stage – a small detector package of 13mm x 13mm, able to patrol the required image plane. In normal operation the YJ and RI cameras have a 3 mm thick long-pass filter and the H camera has a 0.3 mm thick silicon filter a short distance before the image plane. To mimic this a 3 mm thick N-BK7 window was installed in front of the XIMEA camera for the YJ and RI cameras. The XIMEA camera also has a 0.4 mm protective window just in front of the detector.

The first step in the fine alignment and testing procedure on the test bench was to take Hartmann images at the central field position. Shown in Figure 13 is a typical Hartmann image. Many of the Hartmann spots are unsuitable due to vignetting or being faint/distorted. A total of 22 spots as indicated were used in the analysis. Spot selection is symmetrical about the horizontal and vertical axis through the centre of the image. A Zemax merit function was generated based on the measured positions of the Hartmann spots. The design was then optimised with the lens-mirror spacing, lens tilts and decentres and rotation in the focal plane as variables. The three adjustment motors were used to bring the tilts and separation of the lens to the mirror until within tolerance of the required values (+/- 30 arcseconds in tilt, and 0.05 mm separation).

The second step is to acquire in-focus images on a 5x5 grid covering the complete focal plane by translating and refocussing the XIMEA camera. For each image extractions in both the X and Y directions across the fibre image were taken (averaging over 5 pixels). FITYK[4], an open-source curve-fitting package was used to fit a Gaussian curve to the background extracted cut, returning the central position, peak signal and half width at half maximum (HWHM) of the fitted cut. The HWHM in pixels is converted to FWHM in microns using the detector pixel scale. As mentioned earlier, as the test wavelength is 850 nm this is less than ideal for the cameras optimised for the YJ and H wavebands, resulting in a slight broadening of the image profiles compared to the design wavelength profiles.

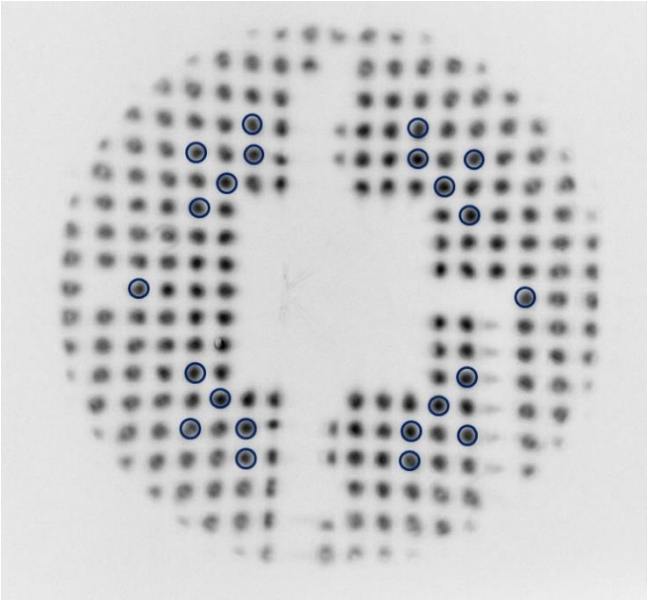

Figure 13 The on-axis Hartmann pattern used to determine the tilts and spacings within the MOONS camera. The 22 spots circled in the image were used in the model fitting.

6.4 Cryogenic alignment in the test rig

The complete test bench was installed into the cryogenic chamber and cooled to operating temperature (128 K) – a ten-day procedure. It had initially been hoped that the change from ambient to cold measurements would be relatively benign (that is the tilt of the lens to the mirror would not change significantly). However, it was clear that this was far from the case, resulting in a significant change in the measured tilts of more than 60 arcseconds. Hence adjustments were required to bring the tilts and separation at operating temperature to within specification. Imaging data were again obtained in a 5x5 grid.

The chamber was warmed to ambient then re-cooled to operating temperature as a check on the stability of the system. No significant change in tilts or separations was found in this procedure.

The system was then warmed to ambient again, the chamber opened, the three adjusters locked and the motors removed. The system was then re-cooled. A further set of Hartmann and imaging data were obtained once stable at operating temperature. For all cameras the locking and motor removal proved to be relatively benign, in that the tilts and separation remaining within tolerance.

A specimen image and X and Y profiles taken with the first RI camera after final lock down and cooling are shown in Figure 14.

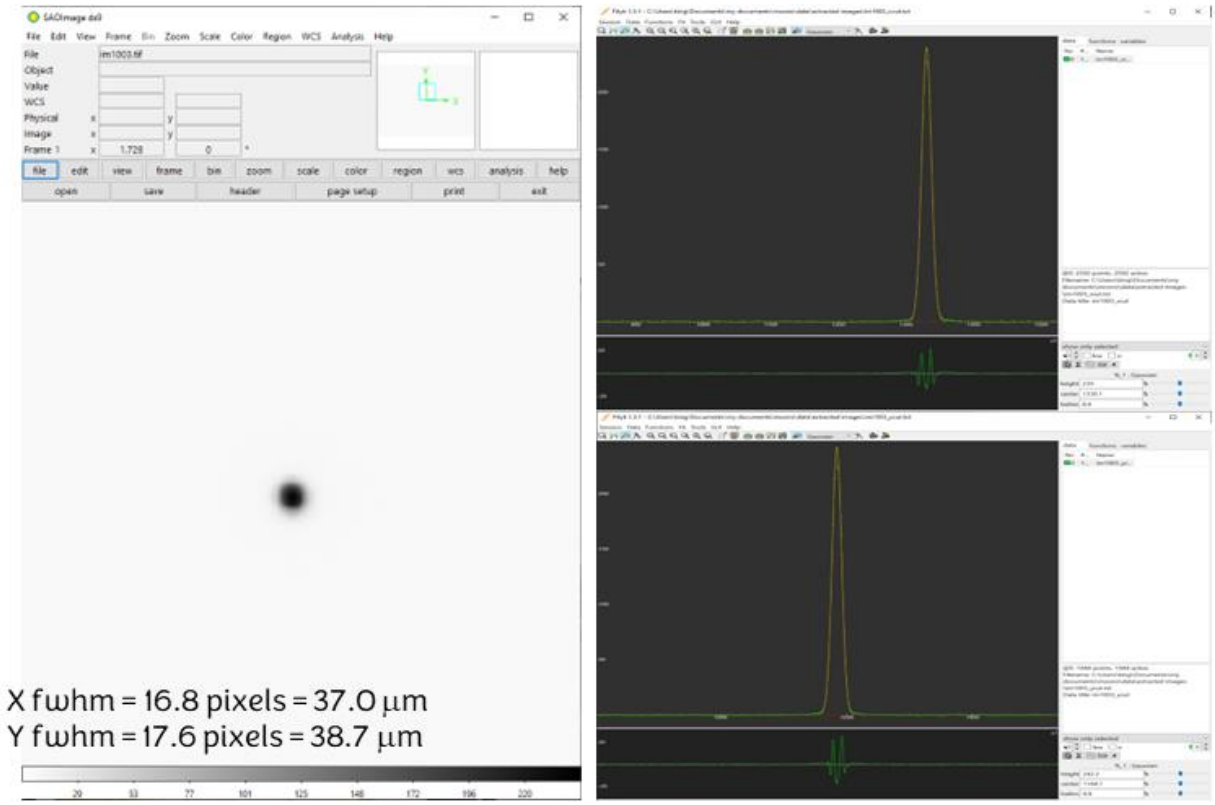

Figure 14 An image, X profile and Y profile of the central fibre of the first RI camera.

6.5 Alignment results

In Table 5 below, are the tilts and separations for each camera as determined by the fit to the appropriate Zemax model for each of the cameras after the three adjusters had been locked and the cryogenic chamber was stable at operating temperature. These values are typically the mean of between 10 and 12 individual Hartmann images. The errors are the standard error of the mean.

Table 5 Tilts and mirror to lens separations measured for the final cooldown for each camera. column 1: camera, columns 2 and 3: tilts, column 4: separation lens to mirror. The Zemax model optimal separation is shown in brackets. Tilt specification is +/- 30 arcsecs, separation is design +/- 0.05 mm.

Camera	Tilt about x (arcsec)	Tilt about y (arcsec)	Separation (mm)	
H s/n 1	-18.40 +/- 3.66	-2.38 +/- 4.19	257.64 +/- 0.02	(257.60)
H s/n 2	16.44 +/- 4.18	6.72 +/- 5.08	257.11 +/- 0.02	(257.13)
RI s/n 1	16.12 +/-3.71	-5.83 +/- 5.31	257.54 +/-0.04	(257.49)
RI s/n 2	15.96 +/- 3.80	-6.88 +/- 4.32	257.58 +/- 0.02	(257.54)
YJ s/n 1	20.08 +/-3.59	-19.16+/- 4.90	259.13 +/-0.02	(259.22)
YJ s/n 2	-7.72 +/- 2.55	12.24 +/- 2.98	259.03 +/- 0.03	(259.07)

The image quality, as determined from the in-focus images, is constant over most of the full image plane, only degrading in the extreme corners. Additionally, the image profiles are slightly broader in the YJ camera and more so in H-band cameras – this is a consequence of tests using the out of band light source and is consistent with the Zemax modelling. The Gaussian fits in the 5x5 grid for the first RI camera about the central field is shown in Table 6.

Table 6 The 5x5 grid covering the image plane of the MOONS RI camera s/n 1. The FWHM in X and Y at the grid position about the central point in the image plane are shown in each box.

Field position	-27.5 mm Fwhm_x(μm) Fwhm_y(μm)	-13.7 mm Fwhm_x(μm) Fwhm_y(μm)	0.0 mm Fwhm_x(μm) Fwhm_y(μm)	13.7 mm Fwhm_x(μm) Fwhm_y(μm)	27.5 mm Fwhm_x(μm) Fwhm_y(μm)
27.5 mm	38.3 47.5	35.6 43.6	35.2 41.3	37.4 43.5	45.8 42.7
13.7 mm	40.0 44.9	37.0 37.4	37.4 40.5	37.4 36.5	39.2 36.1
0.0 mm	37.4 47.0	37.5 42.7	37.0 38.7	37.0 39.6	37.8 40.4
-13.7 mm	37.4 38.3	35.2 38.7	34.3 36.1	36.1 36.1	37.0 37.4
-27.5 mm	39.6 40.5	36.5 37.8	36.1 35.6	40.0 35.6	44.0 38.7

6.6 Summary

An outline of the procedures used to align and test all MOONS spectrograph cameras is presented. For all cameras, the relative tilt between the lens and the mirror, the lens to mirror spacing, and the image quality over the image plane meets the design specification.

7 CAMERA STATIC AND SHOCK LOAD TESTING

The purpose of these tests is two-fold: (1) to measure the displacement of the optics under quasi-static (gravity) loading and obtain an estimate of friction limited displacement to compare the results with the design analysis; (2) to determine the displacement and restoration of the optics under a dynamic load (simulated earthquake loading) and compare the results with the requirements for maintaining camera alignment following and earthquake.

7.1 Camera alignment requirements

The requirements placed on the camera and optics are presented in Table 7 together with the estimated performance derived from analysis of the design. In a direction perpendicular to the optical axis the lens and mirror each may translate by as much as 50 μm in any direction. Hence their relative, or differential, displacement may be as much as 100 μm. The mirror and lens may each translate in the direction of the optical axis by up to 50 μm.

Table 7 Performance requirements of the relative alignment of the camera and its optical elements.

Requirement	Requirement (mm)	Performance Analysis (mm)
Delta-X/Y (mm) perpendicular to optical path:		
Whole camera relative to disperser:	1.0	±0.3
M1 relative to camera assembly:	0.05	0.035 – 0.044
L1/L2 relative to camera assembly:	0.05	0.021 – 0.030
Delta-Z (mm) along optical path:		
Whole camera relative to disperser: 1.0	1.0	±0.3
M1 relative to camera assembly: 0.05	0.05	Less than ±0.02
L1/L2 relative to camera assembly: 0.05	0.05	Less than ±0.02

7.2 Camera performance analysis

Several calculations are presented in the camera performance analysis which are useful references with which to compare test results. These are:

- Decentre values for L1+L2 and the mirror under gravity and in the absence of friction (i.e., due simply to radial spring support). These are 34 μm (L1+L2) and 49 μm (M1)
- The relative displacement between L1+L2 and M1 for each camera in the absence of friction at their operating orientations (angle from axis horizontal). These are: 5.3 μm for H (at 38°); 4.3 μm for YJ (at 13.6°) and 7.0 μm for RI at 8°.
- The worst-case de-centring error due to friction at the interface between the optical surfaces and their mounts is (averaging the three cameras) 20 μm for the lens and 28 μm for the mirror.
- The worst-case relative displacements between lens and mirror when friction is included is then 14.3 μm for the H camera, 12.8 μm for the YJ camera and 15 μm for the RI camera.

The camera design was identical for all cameras except for shimming based on metrology of component diameters. Deflections of each optical element expected under gravitational loading for the operating orientation of the camera are in Table 8. The differential displacement between lens and mirror is expected to be <10 μm (in the absence of friction).

Table 8 Expected (calculated) differential optical component deflections under gravity at their operating orientation.

Camera	H	YJ	RI
Angle of optical axis from horizontal in operation	38°	13.6°	8°
Lateral differential displacement of lens/mirror without friction	5.3 μm	4.3 μm	7 μm
Worst-case differential displacement lens/mirror including friction	14.3 μm	12.8 μm	15 μm

7.3 Quasi-static testing

The purpose of quasi-static testing is to check that the actual deflections of each optic are consistent with the expected deflection under gravity loading. In addition, the effect of friction can be estimated from the apparent hysteresis in the deflection measurements.

The camera was fitted with eight displacement sensors, four on the lens cell and four on the mirror cell. The sensors have an accuracy of 1 μm and measure the displacement of the optic with respect to the cell. The camera is then tilted from a position where the optical axis is vertical to one where the optical axis is horizontal and at the operating orientation, as shown in Figure 15 (left). Repeated cycles of this operation provided the information required to verify the expected performance.

The RI camera was tested for translations of lens and mirror under gravitational load change between (optical) axis vertical and axis horizontal. After ensuring that the lens and mirror were centred within the limits that friction would allow the results shown in Table 9 were obtained. These show that the differential displacement between axes of the lens and mirror are <7 μm, better than expected. With its axis vertical the camera was shaken to establish position hysteresis due to friction.

Table 9 Measured optical component deflections of the RI camera under full gravitational load.

Optical axis	Lens (μm)	Mirror (μm)	Differential (μm)
Vertical	0	0	0
Horizontal	-23.6	-30.1	6.5
Vertical	-15.2	-20.5	5.3
Inferred effect of friction	8.4	10.5	-
Position hysteresis with the axis vertical	11.6	10.2	-

Figure 15 The arrangements for camera load testing: **left**, the quasi-static deflection of camera optics under gravitational loading, and **right**, the impulse test arrangement showing the camera mounted to a base-plate fitted with compliant feet.

7.4 Dynamic testing

To test the dynamic response of the optics the camera is attached (via its standard fixings) to a base-plate which is supported on flexible machine isolation mounts. The base-plate is manually struck by a weight through a soft pad such that an impulse is imparted in a desired direction. The resulting accelerations are monitored by a three-axis accelerometer secured to the centre of the base-plate and another single axis accelerometer mounted on the camera and aligned to the desired direction. The displacement sensors also record displacement of the optics in the mirror and lens cell to indicate how well the optic re-centres after a disturbance. The resilient mounts produce a characteristic frequency of ~10 Hz and the soft pad allows a broad profile impulse which creates sufficient excitation at low and moderate frequencies to produce motion of the optics within their cells. To achieve a vertical impulse without striking the camera directly the baseplate was raised above the testbed by 10 cm at one end and then allowed to drop. This produced an impulse through the camera support mount of greater than 2.5g which was a test requirement for a camera.

For the dynamic tests, a series of impulses were applied and the response of the accelerometers logged. The positions of the optics were recorded after each test so that any change in rest position can be determined. These results are consistent with the results obtained in the static tests and, in fact, are rather better because the oscillatory response has the effect of reducing the static friction dead-band. For the final series of tests, the single axis accelerometer channel was exchanged for the average displacement of the mirror in the vertical or horizontal direction to capture the motion of the mirror during each test. The dynamic response from some of these tests are shown in Figure 16 (left), which is the response from a vertical impulse delivered to the baseplate by lifting one end and allowing it to drop from about 10cm onto its compliant mounts. The vertical displacement of the mirror (orange) is 57μm pk-pk with breakaway at ~1.2g and settles to within 11 μm. The maximum vertical acceleration is 2.6g. Figure 16 (right), shows the response from a longitudinal impulse delivered to the top of the camera A-frame using a soft tipped mallet and additional damping material. In this case, a peak acceleration of >3g was applied and produced an initial displacement of 50 μm peak. Displacement breakaway occurred at ~3g and motion eventually settled within 1.5 μm of the start position. The impulse also produced a high frequency excitation of ~150 Hz and was probably responsible for the narrower settling band.

These pictures provide a clear picture of motion of the mirror as the acceleration profile decreases and consequently the effect of friction in limiting mirror motion.

These tests adequately demonstrate that the camera remains in alignment after shock loads that might be generated during transportation and comply with the earthquake survival specifications.

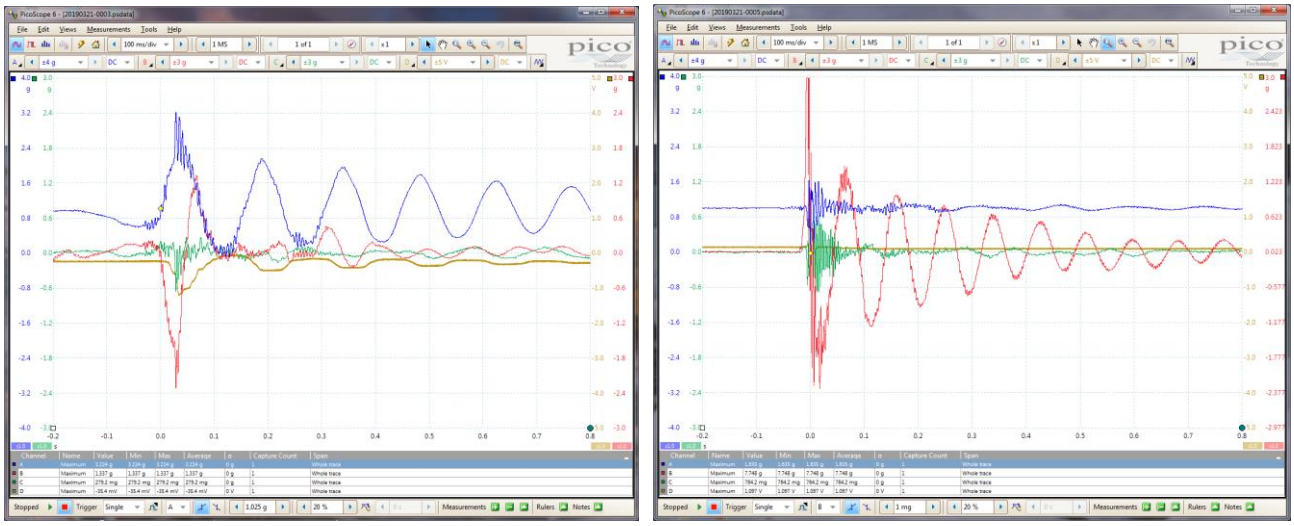

Figure 16 **Left**: response from a vertical impulse delivered to the baseplate by lifting one end and allowing it to drop from about 10cm onto its compliant mounts. From the 3-axis accelerometer on the baseplate: vertical response (blue), axial response (red), and transverse response (green). The vertical displacement of the mirror (orange) is 57μm pk-pk with breakaway at ~1.2g and settling to within 11 μm. The maximum vertical acceleration is 2.6g. **Right**: response from a longitudinal impulse delivered to the top of the camera A-frame using a soft tipped mallet and additional damping material. In this case, a peak acceleration of >3g was applied and produced an initial displacement of 50 μm peak. Displacement breakaway occurred at ~3g and motion eventually settled within 1.5 μm of the start position. From the 3-axis accelerometer on the baseplate: the blue trace is the vertical response (note the 1g offset); the red trace is the longitudinal response and the green trace is the transverse response.

7.5 Summary

The quasi-static and dynamic tests confirm the expected behaviour of the optics within their cell modules. The camera remains in optical alignment because of the way the optical elements are held and defined.

8 CONCLUSIONS

The quality of the optical components, the mechanical design of the camera and the alignment process have been shown to meet expectations through the tests described here. The first camera to be aligned underwent 5 cool-down and warm-up cycles to prove that the alignment was stable but for the remaining cameras, two cycles were judged to be sufficient. All six of the MOONS cameras have now been completed and delivered to the instrument integration site at the UK Astronomy Technology Centre in Edinburgh. Two of the cameras, the RI and YJ, have been integrated into one of the spectrographs in the instrument cryostat and have produced better than required image quality[5]. Recent tests show that the PSFs are good across the whole detector array - at 2.5 to 2.7 pixels FWHM. These results follow transportation, installation and cold cycling of the first two cameras delivered.

REFERENCES

[1] Oliva, E., Todd, S., Cirasuolo, M., Schnetler, H., Lunney, D., et al., 2014. S.P.I.E. 9147, 91472C.
[2] Oliva, E., Delabre, B., Tozzi, A., Ferruzzi, D., Lee, D., et. al., 2016. S.P.I.E. 9908, 9908R.
[3] Li Causi G.*a, Lee D.b, Vitali F.a, Royer F.c, Oliva E. Proceedings of SPIE 99088 2016
[4] Wojdyr, M, 2010. J. Appl. Cryst. 43, 1126.
[5] Martin Black, David Lee, Oscar Gonzalez, Jonathan Strachan, William Taylor. This conference, paper 12184-273